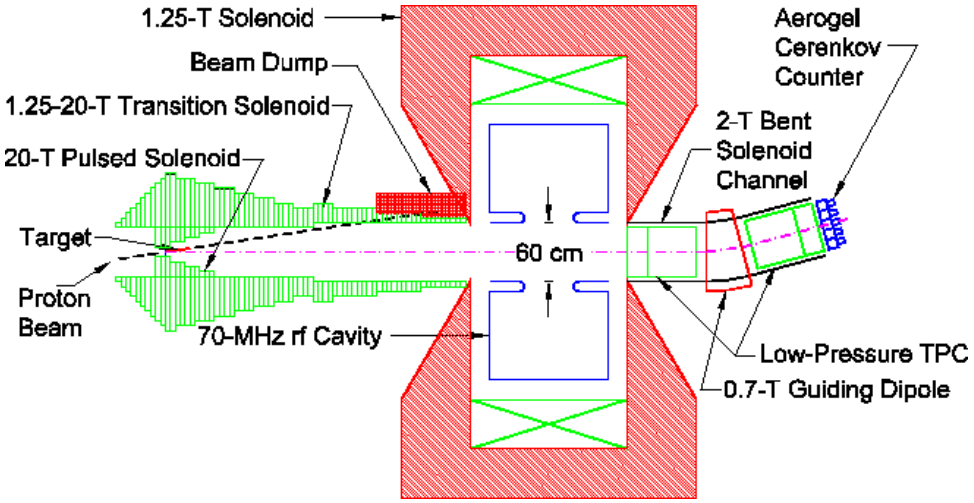

FIG. 22. Plan view of the full configuration of the targetry experiment.

V. IONIZATION COOLING

A. Introduction

The design of an efficient and practical cooling system is one of the major challenges for the muon collider project.

For a high luminosity collider, the 6-D phase space volume occupied by the muon beam must be reduced by a factor of $10^5 - 10^6$. Furthermore, this phase space reduction must be done within a time that is not long compared to the muon lifetime (μ lifetime $\approx 2\ \mu s$). Cooling by synchrotron radiation, conventional stochastic cooling and conventional electron cooling are all too slow. Optical stochastic cooling [139], electron cooling in a plasma discharge [140], and cooling in a crystal lattice [141,142] are being studied, but appear technologically difficult. The new method proposed for cooling muons is ionization cooling. This technique [16,18,20,143] is uniquely applicable to muons because of their minimal interaction with matter. It is a method that seems relatively straightforward in principle, but has proven quite challenging to implement in practice

Ionization cooling involves passing the beam through some material in which the muons lose both transverse and longitudinal momentum by ionization energy loss, commonly referred to as dE/dx. The longitudinal muon momentum is then restored by reacceleration, leaving a net loss of transverse momentum (transverse cooling). The process is repeated many times to achieve a large cooling factor.

The energy spread can be reduced by introducing a transverse variation in the absorber density or thickness (e.g. a wedge) at a location where there is dispersion (the transverse position is energy dependent). This method results in a corresponding increase of transverse phase space and is thus an exchange of longitudinal and transverse emittances. With transverse cooling, this allows cooling in all dimensions.

We define the root mean square rms normalized emittance as

$$\epsilon_{i,N} = \sqrt{\langle \delta r_i^2 \rangle \langle \delta p_i^2 \rangle - \langle \delta r_i \delta p_i \rangle^2}/m_\mu c \tag{22}$$

where r_i and p_i are the beam canonical conjugate variables with $i = 1, 2, 3$ denoting the x, y and z directions, and $\langle ... \rangle$ indicates statistical averaging over the particles. The operator δ denotes the deviation from the average, so that $\delta r_i = r_i - \langle r_i \rangle$ and likewise for δp_i. The appropriate figure of merit for cooling is the final value of the 6-D relativistically invariant emittance $\epsilon_{6,N}$, which is proportional to the area in the 6-D phase space (x, y, z, p_x, p_y, p_z) since, to a fairly good approximation, it is preserved during acceleration and storage in the collider ring. This quantity is the square root of the determinant of a general quadratic moment matrix containing all possible correlations. However, until the nature and practical implications of these correlations are understood, it is more conservative to ignore the correlations and use the following simplified expression for 6-D normalized emittance,

$$\epsilon_{6,N} \approx \epsilon_{x,N} \times \epsilon_{y,N} \times \epsilon_{z,N} \tag{23}$$

Theoretical studies have shown that, assuming realistic parameters for the cooling hardware, ionization cooling can be expected to reduce the phase space volume occupied by the initial muon beam by a factor of $10^5 - 10^6$. A complete

cooling channel would consist of $20-30$ cooling stages, each stage yielding about a factor of two in 6-D phase space reduction.

It is recognized that understanding the feasibility of constructing a muon ionization cooling channel is on the critical path to determining the viability of the whole muon collider concept. The muon cooling channel is the most novel part of a muon collider complex. Steady progress has been made both in improving the design of sections of the channel and in adding detail to the computer simulations. A vigorous experimental program is needed to verify and benchmark the computer simulations.

The following parts of this section briefly describe the physics underling the process of ionization cooling. We will show results of simulations for some chosen examples, and outline a six year R&D program to demonstrate the feasibility of using ionization cooling techniques.

B. Cooling theory

In ionization cooling, the beam loses both transverse and longitudinal momentum as it passes through a material. At the same time its emittance is increased due to stochastic multiple scattering and Landau straggling. The longitudinal momentum can be restored by reacceleration, leaving a net loss of transverse momentum.

The approximate equation for transverse cooling in a step ds along the particle's orbit is [13,18,20,24,144,145]

$$\frac{d\epsilon_N}{ds} = -\frac{1}{\beta^2}\frac{dE_\mu}{ds}\,\frac{\epsilon_N}{E_\mu} + \frac{\beta_\perp (0.014GeV)^2}{2\beta^3 E_\mu m_\mu\, L_R}, \tag{24}$$

where β is the normalized velocity, E_μ is the total energy, m_μ is the muon mass, ϵ_N is the normalized transverse emittance, $\beta_\perp$ is the betatron function at the absorber, dE_μ/ds is the energy loss per unit length, and L_R is the radiation length of the material. The betatron function is determined by the strengths of the elements in the focusing lattice [146]. Together with the beam emittance this function determines the local size and divergence of the beam. Note that the energy loss dE_μ/ds is defined here as a positive quantity, unlike the convention often used in particle physics. The first term in this equation is the cooling term, and the second describes the heating due to multiple scattering. The heating term is minimized if $\beta_\perp$ is small (strong-focusing) and L_R is large (a low-Z absorber).

The minimum, normalized transverse emittance that can be achieved for a given absorber in a given focusing field is reached when the cooling rate equals the heating rate in Eq. 24

$$\epsilon_{N,min} = \frac{\beta_\perp (14MeV)^2}{2\beta m_\mu \frac{dE_\mu}{ds} L_R} \tag{25}$$

For a relativistic muon in liquid hydrogen with a betatron focusing value of 8 cm, which corresponds roughly to confinement in a 15 T solenoidal field, the minimum achievable emittance is about 340 mm-mrad.

The equation for energy spread is [18,24,25]

$$\frac{d(\Delta E_\mu)^2}{ds} = -2\,\frac{d\left(\frac{dE_\mu}{ds}\right)}{dE_\mu}\langle(\Delta E_\mu)^2\rangle + \frac{d(\Delta E_\mu)^2_{\text{stragg.}}}{ds} \tag{26}$$

where the first term describes the cooling (or heating) due to energy loss, and the second term describes the heating due to straggling. ΔE_μ is the rms spread in the energy of the beam.

Ionization cooling of muons seems relatively straightforward in theory, but will require extensive simulation studies and hardware development for its optimization. There are practical problems in designing lattices that can transport and focus the large emittance beam. There will also be effects from space charge and wake fields.

We have developed a number of tools for studying the ionization cooling process. First, the basic theory was used to identify the most promising beam properties, material type and focusing arrangements for cooling. Given the practical limits on magnetic field strengths, this gives an estimate of the minimum achievable emittance for a given configuration. Next, the differential equations for cooling and heating described above were incorporated into a computer code. Allowance for the shifts in the betatron phase advance due to space charge and aberrations was included. This code was used to develop an overall cooling scenario, which broke the cooling system into a number of stages, and determined the properties of the beam, radio frequency (rf) cavities, and focusing lattice at each stage.

Finally, several tracking codes were either written or modified to study the cooling process in detail. Two new codes (SIMUCOOL [147], and ICOOL [148,149]) use Monte Carlo techniques to track particles one at a time through the cooling system. All the codes attempt to include all relevant physical processes to some degree, (e.g. energy loss,

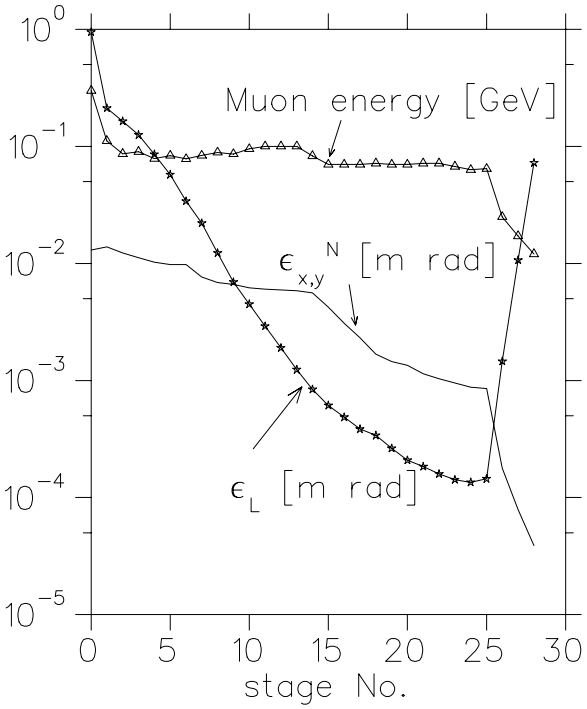

FIG. 23. Transverse ($\epsilon_{x,y}$), longitudinal emittance (ϵ_L) and beam energy *vs.* stage number in the cooling sequence.

straggling, multiple scattering) and use Maxwellian models of the focusing fields. They do not yet take into account any space charge or wake field effects. In addition, we have also used a modified version of PARMELA [150] for tracking, which does include space charge effects, and a double precision version of GEANT [151,152].

We have recently developed [153] a model of beam cooling based on a second order moment expansion. A computer code solving the equations for transverse cooling gives results that agree with tracking codes. The code is being extended to include energy spread and bends. It is very fast and is appropriate for preliminary design and optimization of the cooling channel. All of these codes are actively being updated and optimized for studying the cooling problem.

C. Cooling system

The cooling is obtained in a series of cooling stages. Each stage consists of a succession of the following components:

- Transverse cooling sections using materials in a strong focusing (low $\beta_\perp$) environment alternated with linear accelerators.
- Emittance exchange in lattices that generate dispersion, with absorbing wedges to reduce momentum spread.
- Matching sections to optimize the transmission and cooling parameters of the following section.

The question of the best energy to use for cooling has been discussed in detail in reference [154]. For the set of parameters of interest, a kinetic energy close to 100 MeV appears optimal. At higher energies, weaker focusing raises the heating term from Coulomb scattering, and more acceleration is required for a given amount of cooling. At lower energies, the beam divergence become large, and the rise of $\frac{dE}{dx}$ with falling energy causes a greater increase in energy spread. There can be an advantage, initially, of using a somewhat higher energy to reduce the beam dimensions and bucket length; at the end, the energy can be dropped to attain the lowest transverse emittances at the expense of longitudinal emittance. In the examples that follow it is seen that the simulated transverse cooling stages lower the 6-D emittance by a factor of about 2. Since the required total 6-D cooling is $O(10^6)$, about 20 such stages are required.

We have performed calculations of complete cooling systems for the Higgs factory and for a high energy collider. These calculations are based on theoretical models of the expected cooling performance. They give an indication of

the system dimensions, magnet strengths, rf frequencies and gradients, and beam parameters that will be required in a cooling system. The calculations suggest that the required cooling for a Higgs factory could be achieved in 25 stages, while the high energy collider would require 28 stages. Emittances and energies as a function of stage are shown in Fig. 23. The sequence can be considered to consist of 3 parts:

1. For the first 12 stages the primary effort is to cool in the longitudinal direction in order to reduce the bunch lengths and allow higher frequency rf to be employed. Some transverse cooling is needed in order to reduce the transverse dimensions of the beam and allow it to fit through the smaller irises at the higher frequencies. In this example, for the first stage, an energy of 300 MeV was used to calculate the reduction on the momentum spread and transverse beam dimensions. It is recognized that designing an emittance exchange at the beginning of the system that can simultaneously accept the large initial phase space of the beam and reduce the longitudinal emittance will be a major challenge. In later stages the energy is closer to 100 MeV. Solenoid focusing was assumed in all stages, with an initial field of the order of 1 T rising to about 3 T at the end.

2. In the second part (in this example, stages 13 - 25) the 6-D emittance is reduced as far as possible. For the case of a low momentum spread Higgs collider, the required beam parameters are now achieved and the third part is not required. In this example, 80 MeV energy was used for all stages. Solenoid focusing was used in all but the last two stages, where lithium lenses were assumed.

3. For the higher luminosity and higher energy colliders, further reduction in transverse emittance is required, but this can be obtained without reduction of the 6-D phase space, by allowing the longitudinal phase space to grow. This exchange of emittances is, in this example, achieved by reducing the energy to near 10 MeV in two long lithium lens cooling stages. The same effect could probably be achieved at similar energy, by using a hydrogen absorber with solenoid focusing. It might also be possible by using wedges.

The total length of the system would be of the order of 600 m, and the total acceleration required would be approximately 6 GeV. The fraction of muons remaining at the end of the cooling system is estimated to be $\approx 60\%$. It must be emphasized that this sequence was derived without simulation of the individual stages. It serves however to guide the choice of stages to study in detail.

Three transverse cooling examples have been designed and simulated. The first uses 1.25 T solenoids to cool the very large emittance beam coming from the phase rotation channel. The muon beam at the end of the decay channel is very intense, with approximately 7.5×10^{12} muons/bunch, but with a large normalized transverse emittance ($\epsilon_{x,N}$(rms) $\approx 15 \times 10^3$ πmm-mrad) and a large normalized longitudinal emittance ($\epsilon_{z,N}$(rms) ≈ 612 πmm). The second example would lie toward the end of a full cooling sequence and uses 15 T solenoids. The third example, using 31 T solenoids, meets the requirements for the Higgs factory and could be the final cooling stage for this machine.

The baseline solution for emittance exchange involves the use of bent solenoids to generate dispersion and wedges of hydrogen or LiH to reduce the energy spread. A simulated example is given for exchange that would be needed after the 15 T transverse cooling case.

A lithium lens solution may prove more economical for the final stages, and might allow even lower emittances to be obtained. In this case, the lithium lens serves simultaneously to maintain the low $\beta_\perp$, and provide dE/dx for cooling. Similar lenses, with surface fields of 10 T, were developed at Novosibirsk (BINP) and have been used, at low repetition rates, as focusing elements at FNAL and CERN [7,156–159]. Lenses for the cooling application, which would operate at 15 Hz, would need to employ flowing liquid lithium to provide adequate thermal cooling. Higher surface fields would also be desirable.

Studies have simulated cooling in multiple lithium lenses, and have shown cooling through several orders of magnitude [11]. But these studies have, so far, used ideal matching and acceleration. Cooling is also being studied in beam recirculators, which could lead to reduction of costs of the cooling section [160,161], but full simulations with all higher order effects have not yet been successfully demonstrated.

D. 15 T solenoid transverse cooling example

The lattice consists of 11 identical 2 m long *cells*. In each cell there is a liquid hydrogen absorber (64 cm long, 10 cm diameter) in the 15 T solenoid focusing magnet (64 cm long, 12 cm diameter). The direction of the fields in the magnets alternates from one cell to the next. Between the 15 T solenoids there are magnetic matching sections (1.3 m long, 32 cm inside diameter) where the field is lowered and then reversed. Inside the matching sections are short, 805 MHz, high gradient (36 MeV/m) linacs. Figure 24 shows the cross section of one cell of such a system, together with the betatron function, and the magnetic field along the axis. For convenience in modeling, the section shown in Fig. 24(a) starts and ends symmetrically in the middle of hydrogen absorber regions at the location of the

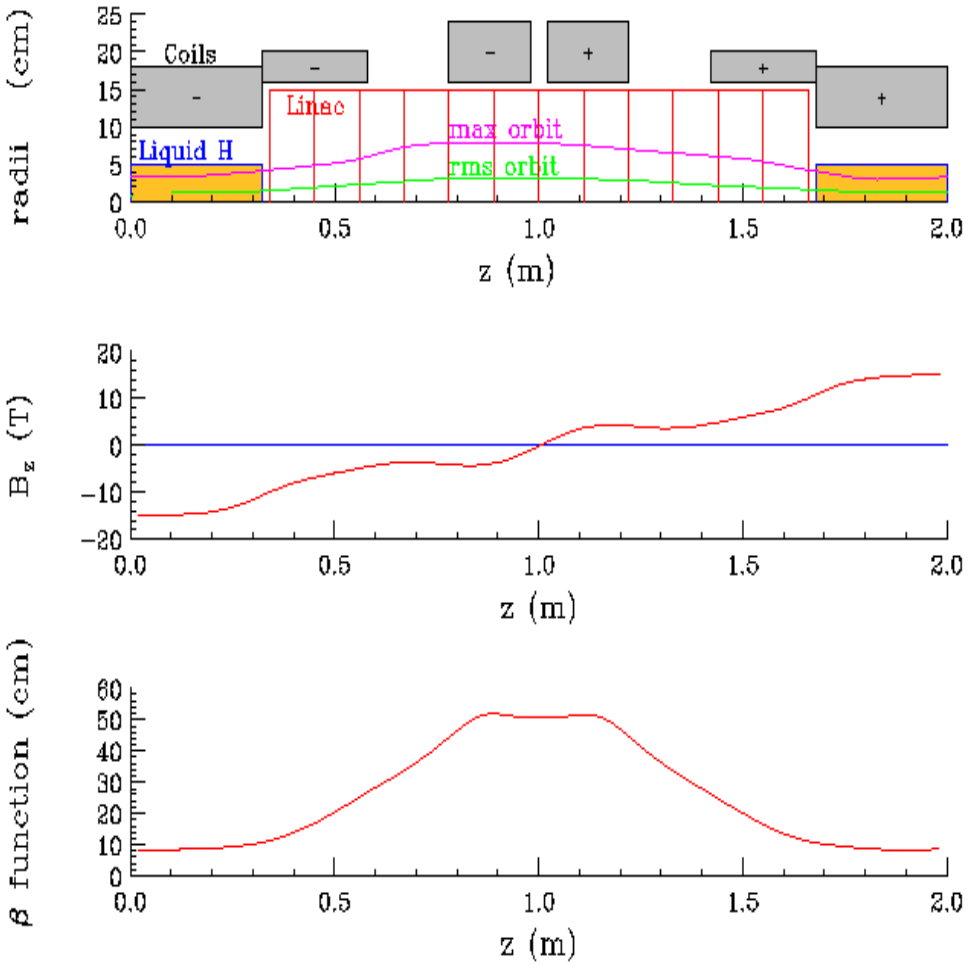

FIG. 24. (a) Cross section of one half period of an alternating solenoid cooling lattice; (b) axial magnetic field *vs.* z; (c) $\beta_\perp$ function *vs.* z.

peaks in the axial magnetic field. In practice each cell would start at the beginning of the hydrogen region and extend to the end of the rf module.

A GEANT simulation of muons traversing a section of the cooling channel is shown in Fig. 25.

Additional simulations were performed [155,162] using the program ICOOL. The only likely significant effects which are not yet included are space charge and wakefields. Analytic calculations for particle bunches in free space indicate that these effects should, for the later stages, be significant but not overwhelming. A full simulation must be done before we are assured that no problems exist. Particles are introduced with transverse and longitudinal emittance (186 MeV/c, 1400 π mm-mrad transverse, and 1.1 π mm longitudinal), together with a number of naturally occurring correlations. Firstly, the particles are given the angular momentum appropriate for the starting axial magnetic field. Secondly, particles with large initial radius r_o and/or divergence θ_o have longer pathlengths in a solenoidal field and tend to spread out with time. This can be parameterized by defining an initial transverse amplitude

$$A^2 = \frac{r_o^2}{\beta_\perp^2} + \theta_o^2. \tag{27}$$

The temporal spreading can be minimized by introducing an initial correlation between p_z and A^2 that equalizes the forward velocity of the initial particles. This correlation causes the average momentum of the beam to grow from the reference value of 186 MeV/c to $\approx$ 195 MeV/c. Lastly, a distortion of the longitudinal bunch distribution can be introduced to reflect the asymmetric nature of the "alpha"-shaped rf bucket.

Figure 26(a) shows the average momentum of the beam as a function of distance along the channel. The momentum drops as the beam crosses the liquid hydrogen absorbers. The gradient and phase of the rf cavities have been adjusted so that the reacceleration given to the reference particle equals the mean energy loss. This causes the average momentum of the beam to remain in a narrow band around 195 MeV/c. Figure 26(b) shows the mechanical and

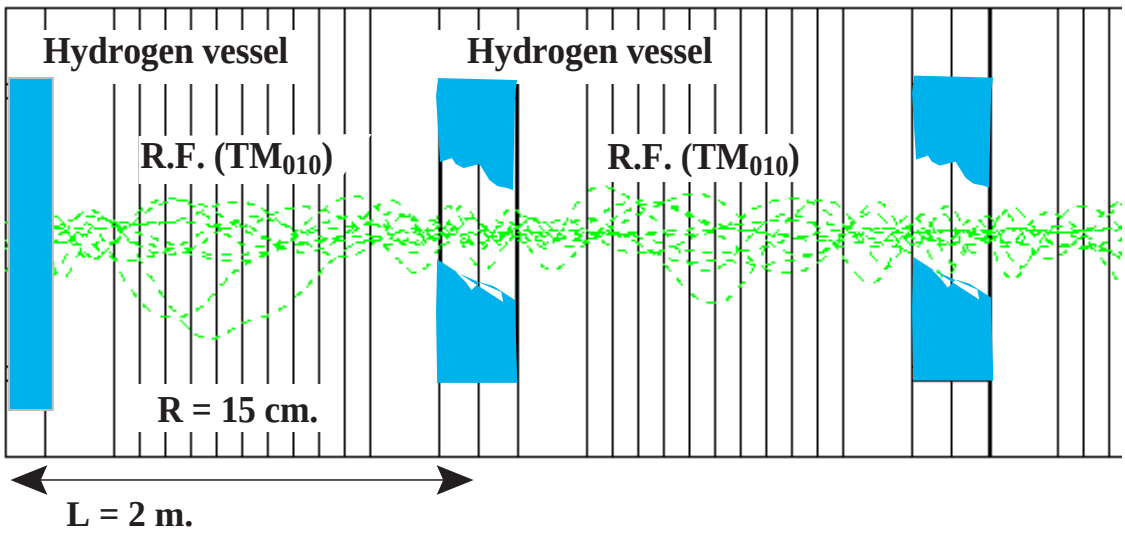

FIG. 25. GEANT simulation of muons traversing a section of the alternating solenoid cooling channel. The variation of the magnetic field B_z is shown for $1\frac{1}{2}$ cells of the figure.

canonical angular momenta as a function of distance along the channel. The mechanical angular momentum shows the rotational motion of the beam around the axial solenoidal field. It periodically reverses sign when the solenoids alternate direction. The canonical angular momentum is defined such that it removes the axial field dependence [162]. Without the absorbers, the beam would have a constant (0) value for the canonical angular momentum. However, the presence of absorbers causes the canonical angular momentum to grow and would lead to severe emittance growth by the end of a long channel. This growth is stopped by alternating the direction of the solenoid field, as shown in Fig. 26(b) Simulations have shown that 2 m is a reasonable (half) period for the field, since the net growth in canonical angular momentum is small. In addition synchrobetatron resonances are avoided since the periodicity of the field forces the average betatron wavelength to be 2 m, whereas the synchrotron oscillation wavelength seen in the simulations for this arrangement is ≈ 14 m.

Figure 27(a) shows the rms and maximum radius of any particle in the beam distribution as a function of distance along the channel. The rms radius shows that most of the beam is confined to within 2 cm of the axis. The peak rms radius decreases towards the end of the channel as a result of the cooling. The maximum particle radius is about 8 cm, which determines the radius of the windows required in the rf cavities. Figure 27(b) shows the rms momentum spread corrected for the correlation between p_z and transverse amplitude imposed on the initial particle distribution. The momentum spread grows as a function of distance since the alternating solenoid system only cools the transverse emittance. Figure 27(c) shows the rms bunch length s a function of distance along the channel. Again this grows with distance since this channel does not cool longitudinally.

Figure 28(a) shows the decrease in transverse normalized emittance as a function of distance along the channel. The system provides cooling by a factor of ≈ 2 in both the x and y transverse phase spaces. From the changing slope of the curve we note that the rate of cooling is dropping. This sets ≈ 22 m as the maximum useful length for this type of system. It must be followed by a longitudinal emittance exchange region to reduce the momentum spread and bunch length approximately back to their starting values. Figure 28(b) shows the increase in longitudinal normalized emittance in the channel due to the increase in momentum spread and bunch length. Finally, Fig. 28(c) shows the decrease in the 6-D normalized emittance as a function of distance along the channel. There is a net decrease in 6-D emittance by a factor of ≈ 2 in the channel. Table V gives the initial and final beam parameters.

This simulation has been confirmed, with minor differences, by double precision GEANT [152] and PARMELA [150] codes.

E. 31 T solenoid transverse cooling example

As in the preceding example, the lattice consists of 11 identical 2 m long cells with the direction of the fields in the solenoids alternating from one cell to the next. The maximum solenoidal field is higher (31 T) than in the previous example, but the bore can be smaller ($6 < r < 8$ cm). Several hybrid magnets with at least this field have operated

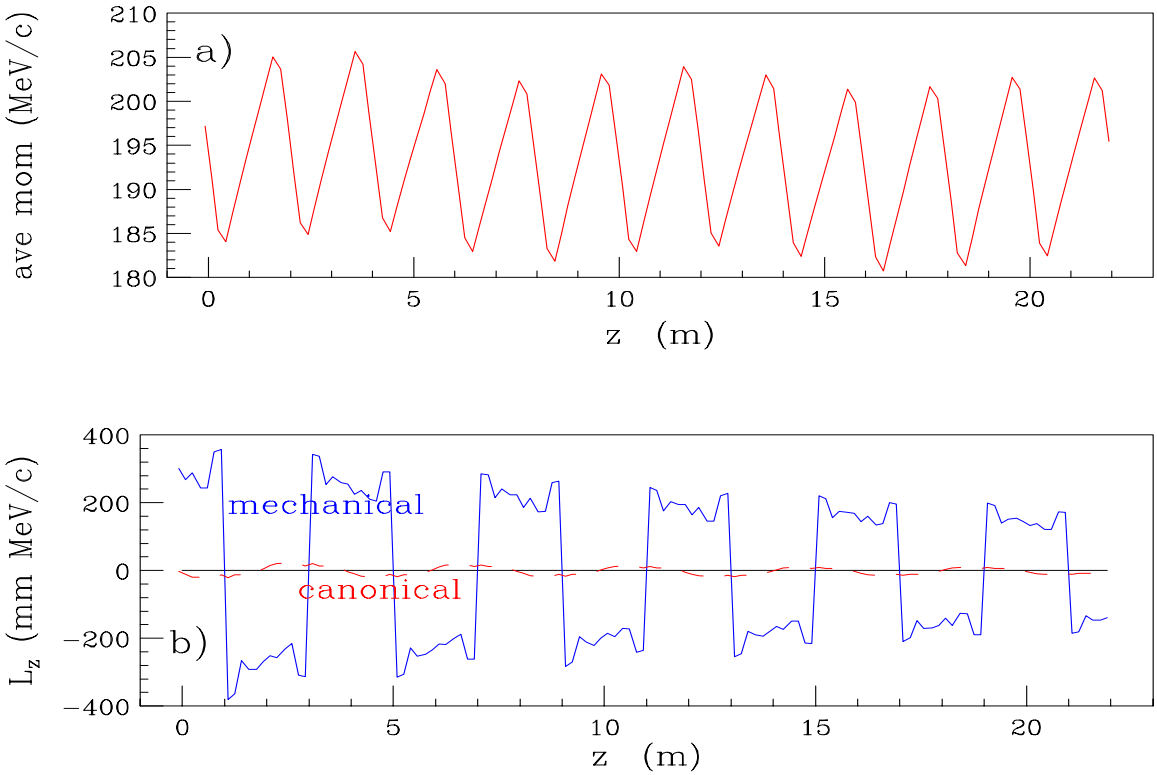

FIG. 26. a) Average momentum *vs.* z; b) Average angular momentum: mechanical (solid curve) and canonical (dashed curve), *vs.* z.

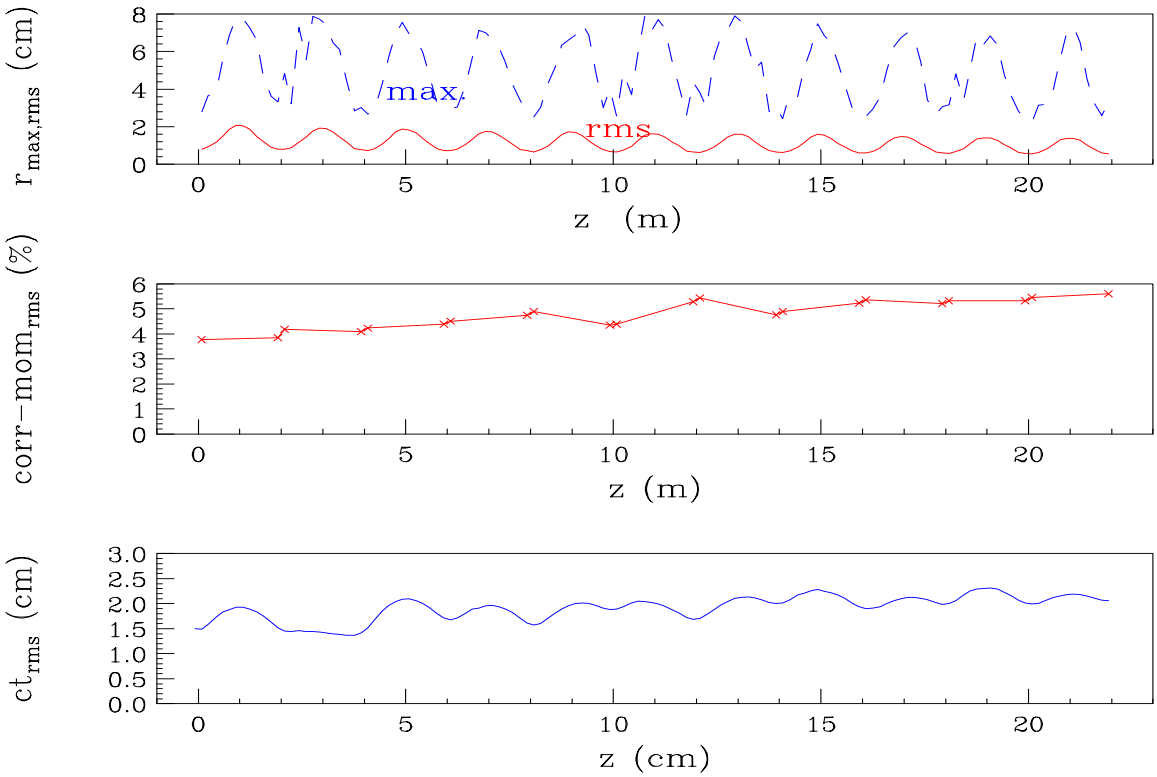

FIG. 27. a) rms and maximum beam radii, b) rms corrected momentum, c) rms bunch length; all *vs.* z.

for many years [163]. More recent magnets are of even higher field. A hybrid solenoid with 45 T central field is under

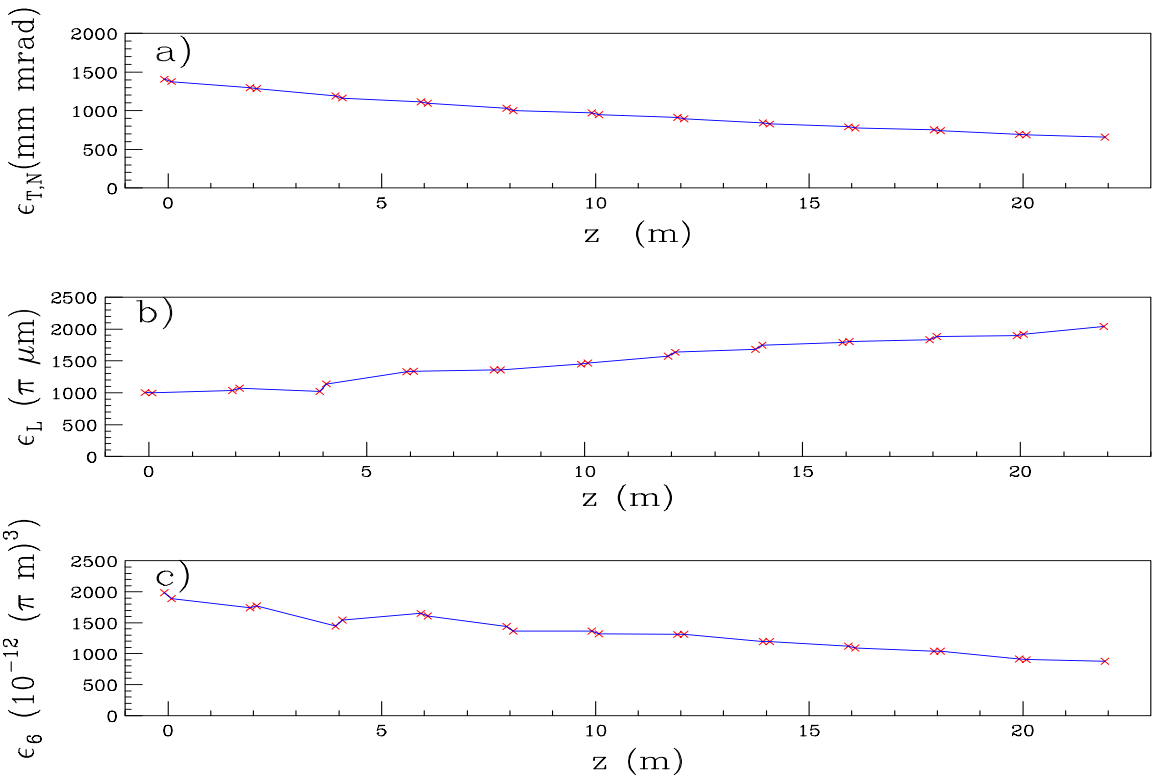

FIG. 28. Emittance *vs.* z: a) transverse emittance $\epsilon_{T,N}(\pi$mm-mrad); b) longitudinal emittance $\epsilon_L(10^{-3}\pi$mm); and c) 6-D emittance $\epsilon_6(10^{-12}\pi\mathrm{m}^3)$.

TABLE V. Initial and final beam parameters in a 15 T transverse cooling section.

		initial	final	final/initial
Particles tracked		1000	980	0.98
Reference momentum	MeV/c	186	186	1.0
Transverse Emittance	π mm-mrad	1400	600	0.43
Longitudinal Emittance	π mm	1.1	2.3	2.09
6-D emittance $\times 10^{-12}$	(π m-rad)^3	2000	800	0.40
rms beam radius in hydrogen	cm	0.8	0.55	0.69
rms beam radius in linac	cm	2.0	1.4	0.70
max beam radius in linac	cm	7.0	7.0	1.0
rms bunch length	cm	1.5	2.2	1.5
max bunch full width	cm	13	19	1.5
rms $\Delta p/p$	%	3.8	5.6	1.5

construction [164]. However, all of these magnets are of small bore and generate their rated field over a length of only a few centimeters. Also, typical hybrid magnet longevity is not adequate for our purposes. 31 T magnets with the needed aperture appear practical, but capital and operating costs are high. High-temperature superconductors are capable of adequate current densities for this field. The challenge is to make them in sufficient lengths and to circumvent their present engineering limitations. If the capital cost of magnets employing high-Tc materials is not prohibitive, and solutions using lithium lenses are not chosen, then high-Tc magnets would be the preferred choice. Between the 31 T solenoids there are 1.3 m long matching sections with an inside diameter of 32 cm, superimposed on a 36 MeV/m reacceleration linac operating at 805 MHz.

Table VI gives the initial and final parameters for the 31 T example, together with the required emittances for a Higgs factory. In setting these requirements a dilution of 20% during acceleration is assumed in each of the three emittances.

TABLE VI. Initial and final beam parameters in a 31 T transverse cooling section.

		initial	final	final/initial	required
Particles tracked		4000	3984	0.99	
Reference momentum	MeV/c	186	186		
Transverse Emittance	π mm-mrad	460	240	0.52	240
Longitudinal Emittance	π mm	0.85	1.6	1.9	
6-D emittance $\times 10^{-12}$	(π m-rad)^3	150	95	0.63	98
rms beam radius in hydrogen	cm	0.44	0.33	0.75	
rms beam radius in linac	cm	.4	1.1	0.80	
max beam radius in linac	cm	6.0	6.0	1.0	
rms bunch length	cm	1.5	1.8	1.2	
max bunch full width	cm	11	19	1.7	
rms $\Delta p/p$	%	3.5	5.0	1.4	

F. Bent solenoid emittance exchange example

We have been considering using a system that exchanges longitudinal and transverse emittance by exploiting dispersion in a large acceptance channel, with a low-Z wedge absorber in the region of dispersion.

In a bent solenoid, in the absence of any dipole field, there is a drift perpendicular to the bend plane of the center of the Larmor circular orbit, which is proportional to the particle's momentum [165,166]. In our example we have introduced a uniform dipole field over the bend to cancel this drift exactly for particles with the reference momentum. Particles with momenta differing from the reference momentum then spread out spatially, giving the required dispersion (0.4 m). The momentum spread is reduced by introducing liquid hydrogen wedges [167]. The hydrogen wedges would be contained by thin beryllium or aluminum foils, but these were not included in this simulation.

After one bend and one set of wedges, the beam is asymmetric in cross section. Symmetry is restored by a following bend and wedge system rotated by 90 degrees with respect to the first. Figure 29 shows a representation of the two bends and wedges. The total solenoid length was 8.5 m. The beam tube outside diameter is 20 cm, and the minimum bend radii is 34 cm.

Figure 30(a) shows the magnetic fields (B_z, B_y, and B_x) as a function of the position along the cell. The solenoid bend curvature is exactly that given by the trajectory of a reference particle (equal in momentum to the average momenta given in Fig. 30(b)) in the given transverse fields. The actual shape of the bend turns out to be very important. Discontinuities in the bend radius can excite perturbations which increase the transverse emittance. We have shown, for example, that the transverse emittance growth in a bent solenoid depends on discontinuities of the bend radius as a function of distance, and its first and second derivatives, the size and tilt of the solenoidal coils, auxiliary fields and the 6-D phase space of the beam. Thus optimization is not straightforward. One solution to this problem is to have long, adiabatic bends. However, this adds undesirable length to the emittance exchange section. We are studying options with coupling sections to tight bends roughly half a Larmor length long, which seems to minimize transverse emittance growth while also minimizing the length of the section. Due to similar problems, the length and longitudinal distribution of the wedge material has also been found to affect emittance growth. For example, the growth can be minimized when the vector sum of the Larmor phases at the absorber elements is small or zero.

The simulations were performed using the program ICOOL. The maximum beam radius is 10 cm. Transmission was 100%. Figure 31(a) shows the rms longitudinal momentum spread relative to the reference momentum as a function of the position along the cell. The fractional spread decreases from an initial value of approximately 5%, to a final value of approximately 2.2%. At the same time, since this is an emittance exchange, the transverse beam area grows, as shown in Fig. 31(b). One notes that the area increases not only in the regions of bends (region 1 and 8), but also in the regions of wedges (2-6 and 9-11). This is probably due to failures in betatron matching that have yet to be understood.

Figure 32 shows scatter plots of the transverse particle positions against their momenta. The dispersion is clearly observed in Fig. 32(b) (after the first bend) and in Fig. 32(e) (after the second). It is seen to be removed, with a corresponding decrease in momentum spread, in Fig. 32(c) (after the first set of wedges) and Fig. 32(f) (after the second set of wedges).

Figure 33 shows a scatterplot of the square of the particle radii vs. their longitudinal momenta, (a) at the start, and (b) at the end of the emittance exchange section. The decrease in momentum spread and rise in beam area are clearly evident.

The initial and final beam parameters are given in Table VII. Although this example demonstrate a factor of ≈ 3

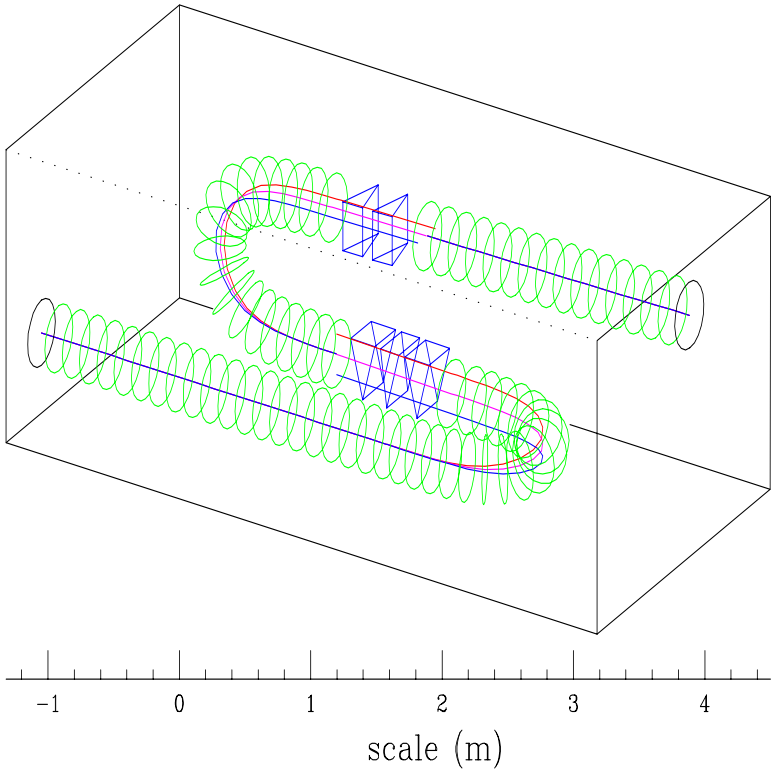

FIG. 29. Representation of a bent solenoid longitudinal emittance exchange section

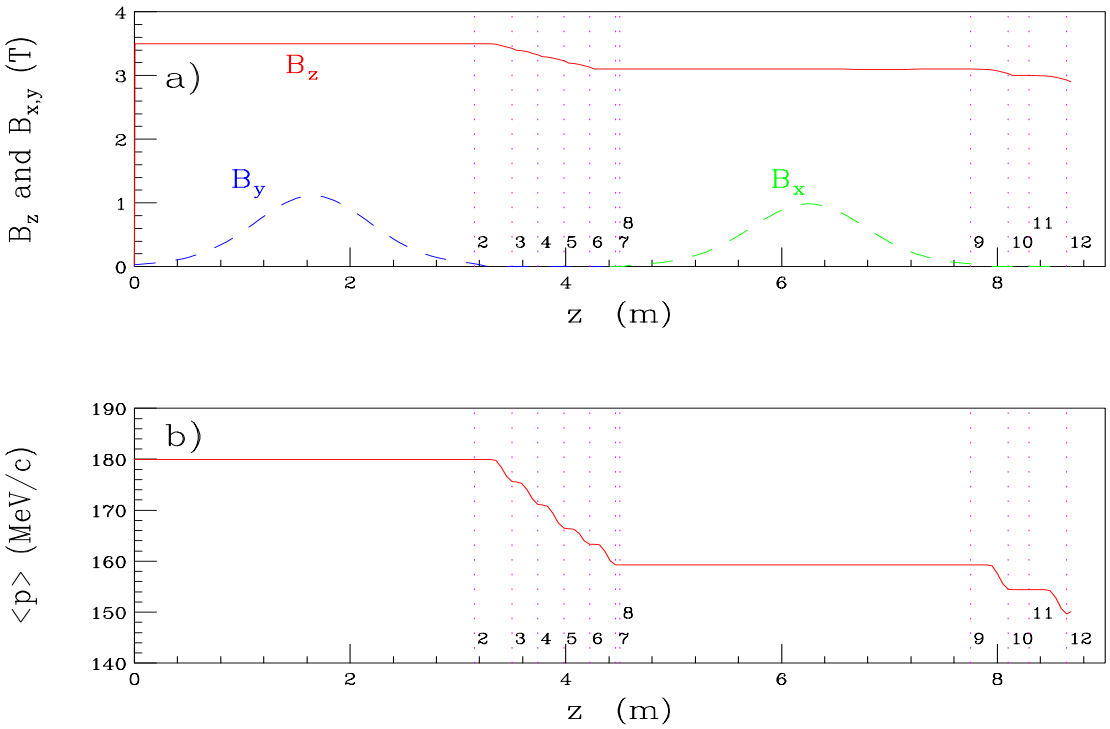

FIG. 30. a) Axial B_z and dipole B_y, B_x, magnetic fields; b) average momentum; both as a function of the position along the cell.

reduction in the longitudinal momentum spread, there is a 37 % increase in the 5-D phase space. The simulations must be extended to include rf so that the 6-D emittance can be studied and the emittance exchange section can be

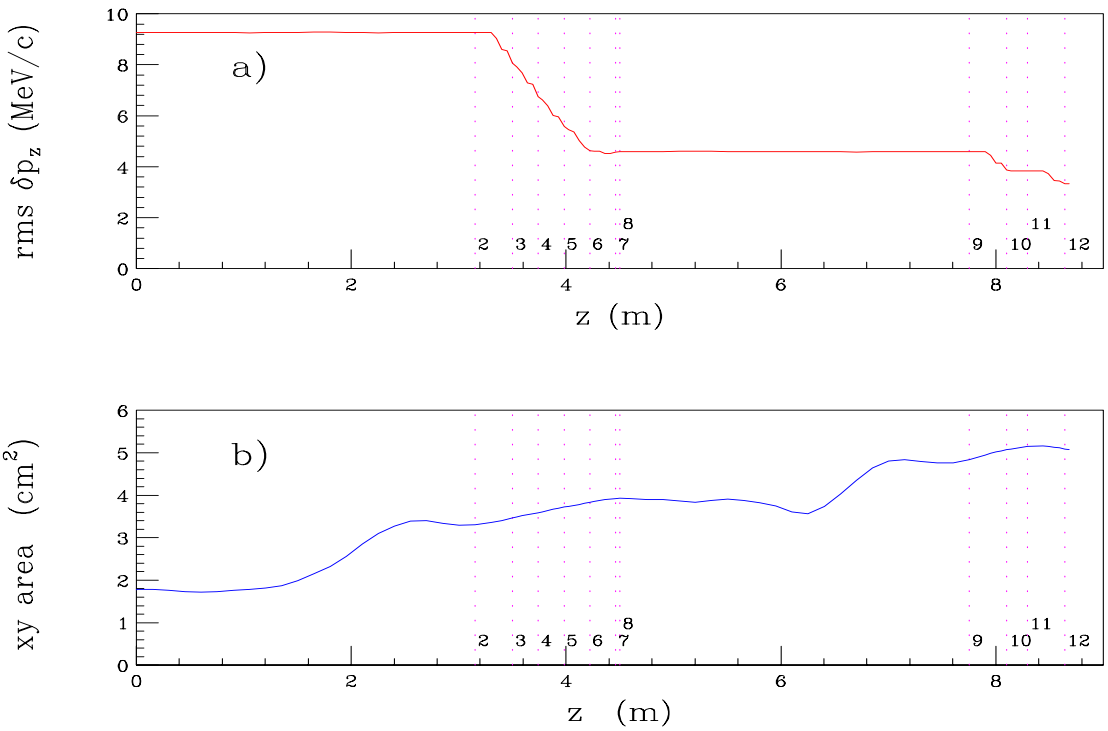

FIG. 31. a) rms longitudinal δp_z with respect to the reference momentum and b) transverse beam area, both as a function of z.

optimized.

TABLE VII. Initial and final beam parameters in a longitudinal emittance exchange section.

		initial	final	final/initial
Longitudinal Momentum spread	MeV/c	9.26	3.35	0.36
Ave. Momentum	MeV/c	180	150	0.83
Transverse size	cm	1.33	2.26	1.70
Transverse Momentum spread	MeV/c	6.84	7.84	1.15
Transverse Emittance	π mm-mrad	870	1694	1.95
$\text{Emit}^2_{\text{trans}} \times \Delta p_{\text{long}}$	(π m-mrad)^2 MeV/c	7.0	9.6	1.37

Emittance exchange in solid LiH wedges, with ideal dispersion and matching, has also been successfully simulated using SIMUCOOL [168]. Dispersion generation by weak focusing spectrometers [160] and dipoles with solenoids [169] have also been studied.

G. rf for the cooling systems

The losses in the longitudinal momentum of the muon beam from the cooling media have to be restored using rf acceleration sections. These rf structures are embedded in solenoidal fields that reverse direction within each section. In the two transverse cooling examples above, the rf frequency is 805 MHz and the peak gradient is 36 MeV/m. The magnetic fields that extend over the cavities vary from 0 to 10 T, reversing in the center. It should be pointed out that in the earlier stages, the bunches are longer, and lower frequencies will be required.

In order to realize maximum accelerating gradients within the acceleration cavities, we take advantage of the penetrating properties of a muon beam by placing thin windows between each rf cell, thereby creating an accelerating structure closely approximating the classic pill-box cavity. This permits operating conditions in which the axial accelerating field is equal to the maximum wall field and gives a high shunt impedance.

The windows in the 15 T example are 16 cm diameter, 125 μm thick Be foils. In the 31 T case, they are 10 cm diameter and 50 μm thick. Two studies indicate that at nitrogen temperature the ohmic losses at the foils are negligible and the mechanical deformation is tolerable. [170]

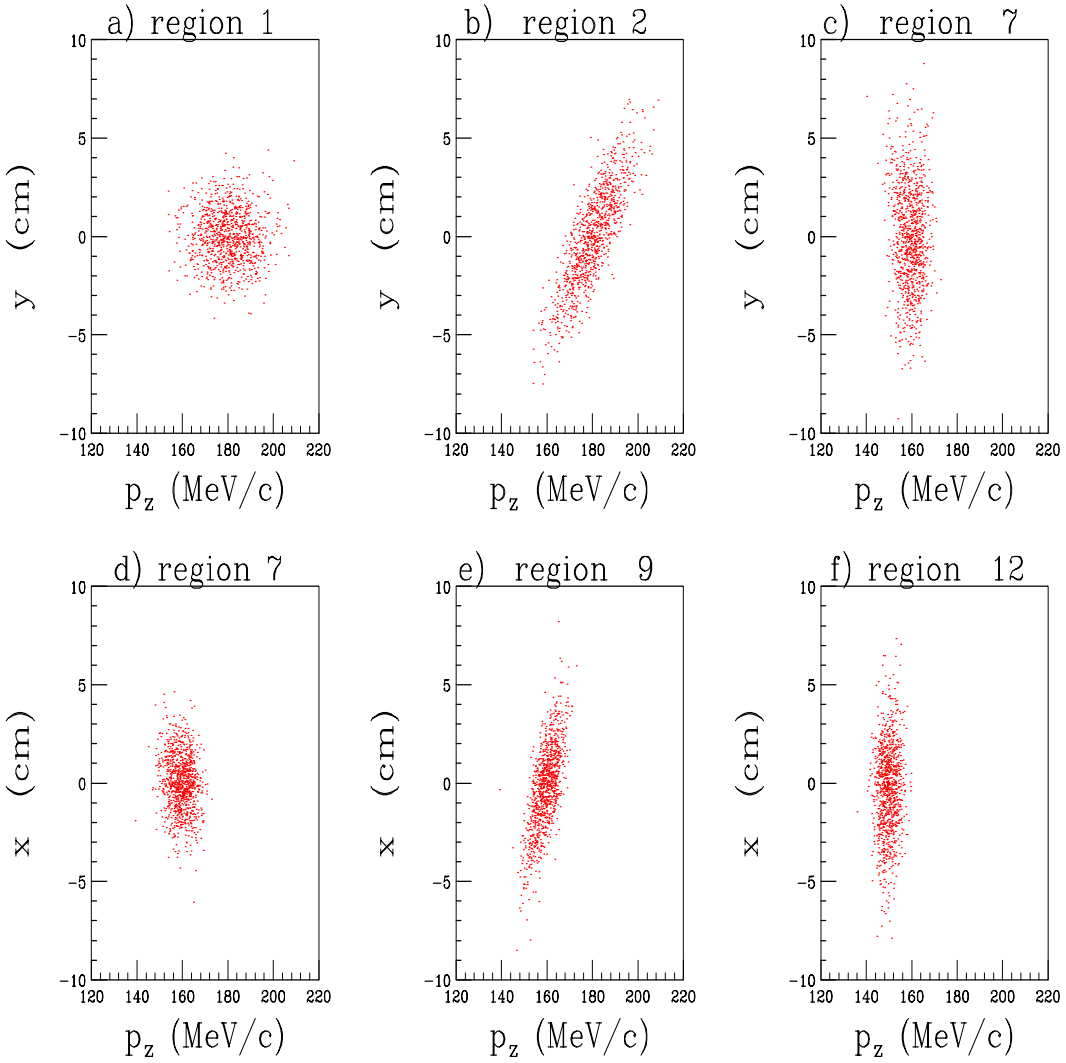

FIG. 32. y *vs.* p_z plots: a) at the start, b) after the first bend, c) after the first set of wedges. x *vs.* p_z plots: d) after the first wedges, e) after the second bend, and f) at the end of the emittance exchange section, following the second set of wedges.

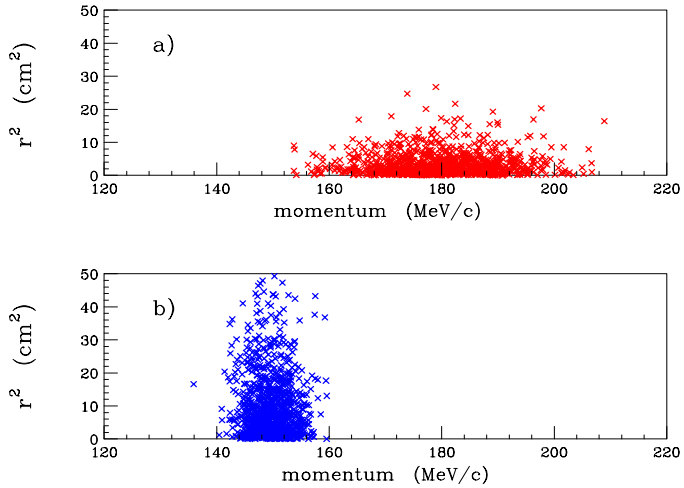

FIG. 33. Scatterplot of squared radii *vs.* longitudinal momentum: a) at the start, and b) at the end of the emittance exchange section.

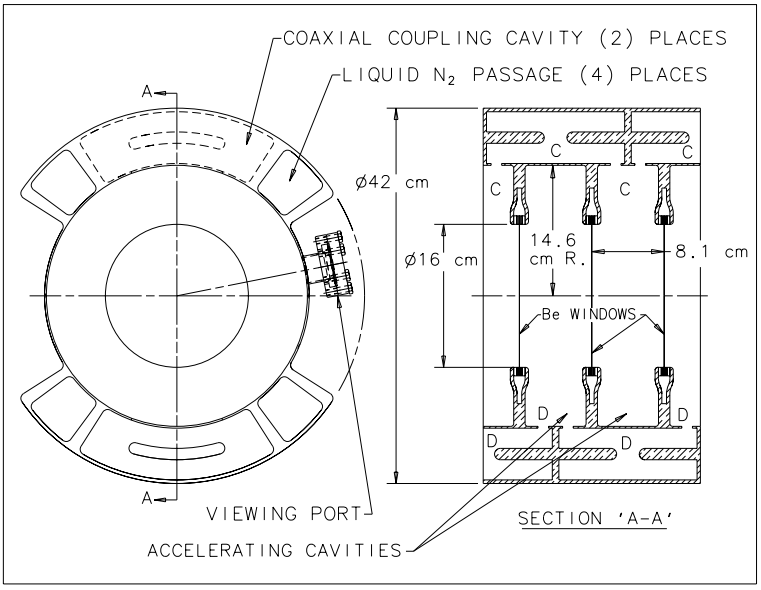

FIG. 34. Two full cell sections plus two half cell sections of the interleaved $\pi/2$ mode accelerating cavities. The volumes labeled **C** are powered separately from the volumes labeled **D**.

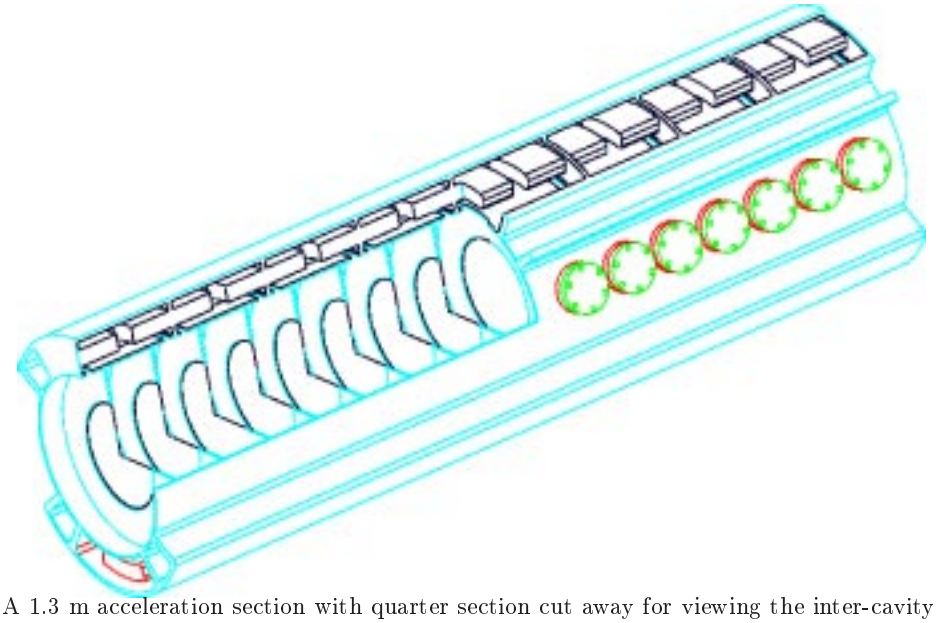

FIG. 35. A 1.3 m acceleration section with quarter section cut away for viewing the inter-cavity windows.

For these rf structures, we will use an interleaved cavity design in which two parts are independently powered (Fig. 34). The mode of the system will be referred to as $\pi/2$ interleaved. Each section supports a standing wave π mode, with each acceleration cell $\pi/2$ long, giving a good transit time factor. To reduce the peak rf power requirements (by a factor of 2), we are considering operating the cells at liquid nitrogen temperatures.

The characteristics of the rf systems currently being studied are summarized in Table VIII. Figure 35 shows a full 1.3 m section with interleaved cavities. Each cell is 8.1 cm in length and the 1.3 m section consists of 16 cells.

TABLE VIII. Characteristics of the rf system.

RF frequency [MHz]	805
Cavity Length [cm]	8.1
Cavity Inner Radius [cm]	14.6
Cavity Outer Radius [cm]	21
$Q/1000$	2×20
Peak Axial Gradient [MV/m]	36
Shunt Impedance [MΩ/m]	2×44
Zt^2 [MΩ/m]	2×36
Fill Time (3 τ) [μs]	2×12
RF Peak Power [MW/m]	$\frac{1}{2} \times 29$
Ave. Power (15Hz) [KW/m]	5.3
Be window aperture [cm]	16 (10 for 31 T case)
Be window thickness [μm]	127 (50 for 31 T case)

H. The liquid lithium lens

The final cooling element ultimately determines the luminosity of the collider. In order to obtain smaller transverse emittance as the muon beam travels down the cooling channel, the focusing strength must increase, i.e. the $\beta_\perp$'s must decrease. A current within a conductor produces an active lens absorber, which can maintain the beam at small $\beta_\perp$ throughout an extended absorber length, while simultaneously attenuating the beam momentum. An active lens absorber, such as a lithium lens, may prove to be the most efficient cooling element for the final stages.

The cooling power of a Li lens is illustrated in Figure 36, where the x *vs.* p_x phase space distributions at the beginning and at the end of the absorber are shown. This example corresponds to a 1 m long lens, with 1 cm radius, and a surface field of 10 T. The beam momentum entering the lens was 267 MeV/c, with Gaussian transverse spatial and momentum distributions: $\sigma_x = \sigma_y = 2.89$ mm, $\sigma_{p_x} = \sigma_{p_y} = 26.7$ MeV/c, and a normalized emittance of $\epsilon_{x,N} = 710$ mm-mrad. The normalized emittance at the end of the absorber was $\epsilon_{x,N} = 450$ mm-mrad (cooling factor ~ 1.57), and the final beam momentum was 159 MeV/c. The results were obtained using a detailed GEANT simulation of a single stage.

An alternative cooling scheme under study uses a series of Li lenses. The lens parameters would have to vary to match the changing beam emittance along the section and in addition, acceleration of the beam between the lenses has to be included.

Lithium lenses have been used with high reliability as focusing elements at FNAL and CERN [7,157,158]. Although these lenses have many similar properties to those required for ionization cooling, there are some very crucial differences which will require significant advances in lens technology: ionization cooling requires longer lenses (~ 1 meter), higher fields ($\sim 10\ T$), and higher operation rates (15 Hz). The last requirement calls for operating the lenses with lithium in the liquid phase. A liquid Li lens consists of a small diameter rod-like chamber filled with liquid Li through which a large current is drawn.

The azimuthal magnetic field focuses the beam to give the minimum achievable emittance $\epsilon_{x,N} \approx C\beta_\perp$ where the constant C depends on the properties of the material, for example, $C_{Li} = 79$ mm-mrad/cm. The focusing term can be written as $\beta_\perp \sim 0.08[\mathrm{cm}]\sqrt{p/J}$ with p is the muon momentum in MeV/c, and J is the current density in MA/cm^2. Increasing J is obviously desirable. Decreasing p can also be useful. However, below about 250 MeV/c the slope of $\frac{dE}{dx}(E)$ tends to increase the longitudinal emittance. The requirement for the highest current density causes large ohmic power deposition. The current density will be limited by the maximum tolerable deposited energy, which will produce instantaneous heating, expansion, and pressure effects. Understanding these effects is part of the ongoing liquid Li lens R&D.

The structural design of the lithium lens is determined by how the pressure pulse and heat deposition are handled. We assume that the Li will be flowing rapidly under high pressure, confined by electrical insulators radially and by fairly thick Be windows longitudinally. Operation at 15 Hz for long periods poses severe challenges. Shock, fatigue and other failure modes are being evaluated, in addition to studies of material compatibilities, corrosion and degradation to insure safe operation over long periods. It seems that the minimum required radius of the lens may be the most important parameter to determine, since mechanical problems increase while losses decrease as a function of radius.

Transferring the beam from one lens to another, with linacs to reaccelerate and provide longitudinal focusing, is also a challenging problem, because of the multiple scattering introduced in the windows, straggling and the large divergence of the beams. We are in the process of evaluating a number of designs for this transfer channel, using detailed tracking simulations that include solenoids, quadrupoles and other focusing elements together with Li lenses.

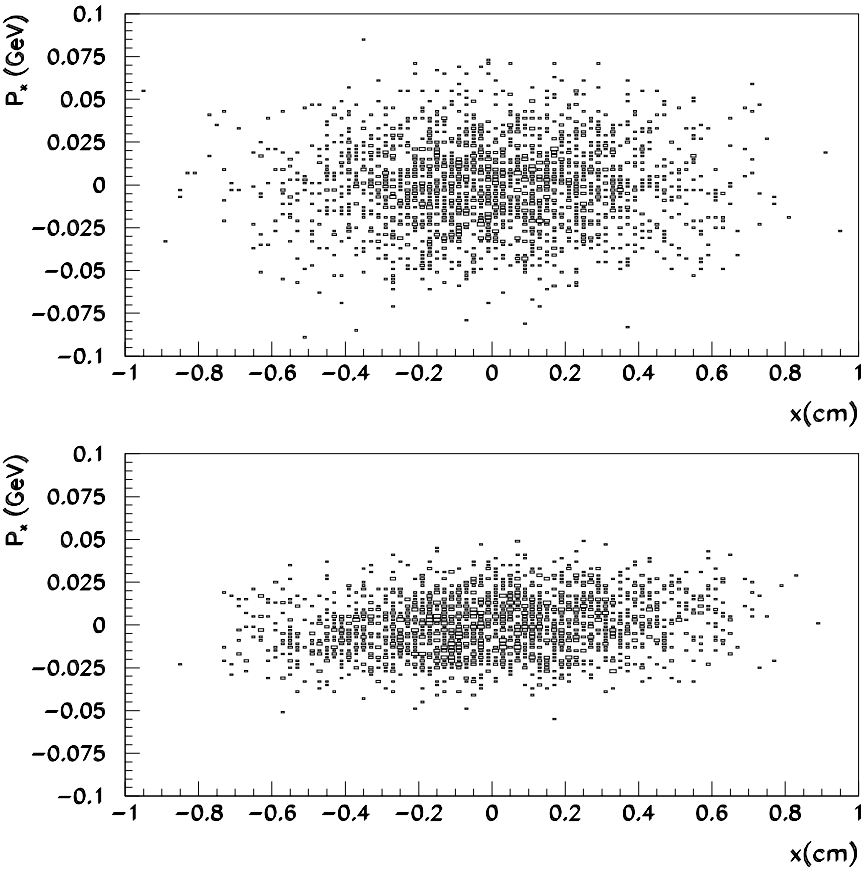

FIG. 36. x-p_x phase space distribution at the beginning (top figure) and at the end (bottom figure) of the absorber described in the text.

A group from BINP has designed, and is constructing, a 15 cm long liquid lithium lens prototype that will eventually be tested at FNAL. It is planned to extend this R&D program to design, construct, and test longer lenses. The design of two lenses, whose behavior will be tested at first on a bench and then with muon beams at the Ionization Cooling Demonstration Facility, will then follow [171].

I. Ionization cooling experimental R&D

An R&D program has been proposed to design and prototype the critical sections of a muon ionization cooling channel. The goal of this experimental R&D program is to develop the muon ionization cooling hardware to the point where a complete ionization cooling channel can be confidently designed for the First Muon Collider. Details can be found in the Fermilab proposal P904 [171]. A summary of the R&D program can be found in ref. [172]. The proposed R&D program consists of:

- Developing an appropriate rf re-acceleration structure. It is proposed to construct a 3-cell prototype rf cavity with thin beryllium windows, which will be tested at high power and within a high-field solenoid.
- Prototyping initially a 2 m section, and eventually a 10 m section, of an alternating solenoid transverse cooling stage. It is proposed to test the performance of these sections in a muon beam of the appropriate momentum.
- Prototyping an emittance exchange (wedge) section and measuring its performance in a muon beam of the appropriate momentum.
- Prototyping and bench testing ~ 1 m long liquid lithium lenses, and developing lenses with the highest achievable surface fields, and hence the maximum radial focusing.
- Prototyping a lithium lens–rf–lens system and measuring its performance in a muon beam of the appropriate momentum.

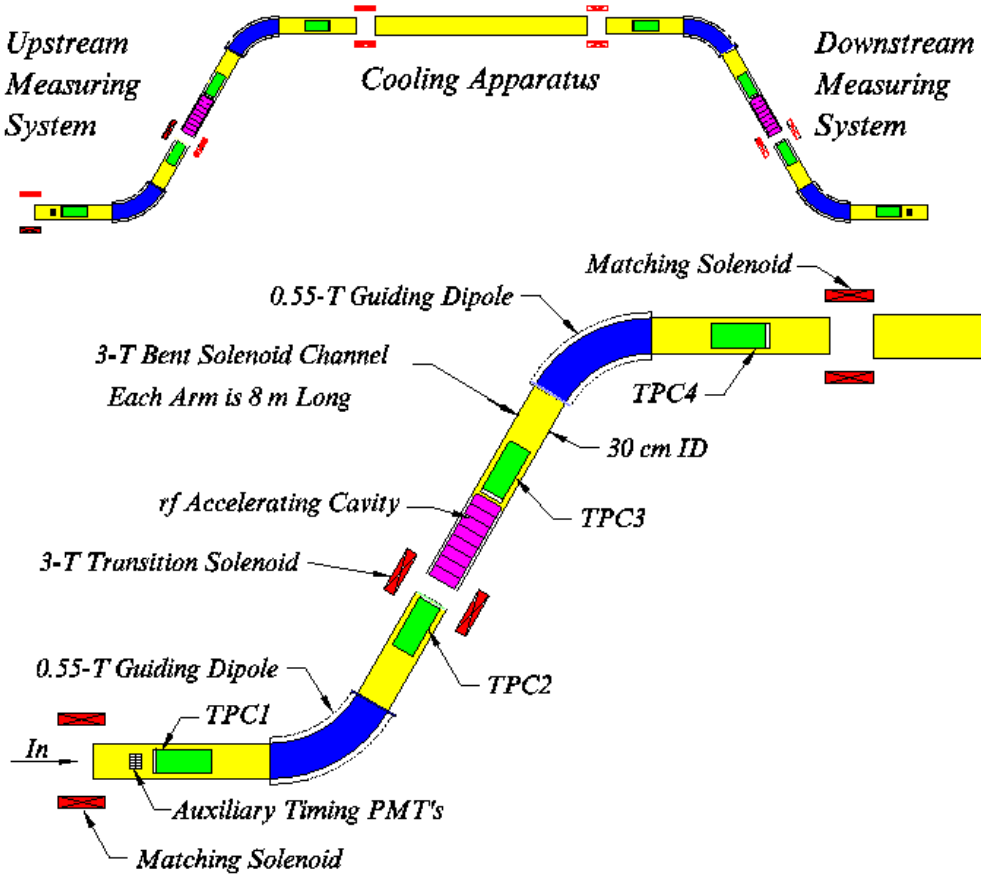

FIG. 37. Schematic of the cooling test apparatus arrangement.

- Developing, prototyping, and testing a hybrid lithium lens/wedge cooling system.

The measurements that are needed to demonstrate the cooling capability and optimize the design of the alternating solenoid, wedge, and lithium lens cooling stages will require the construction and operation of an ionization cooling test facility. This facility will need

1. a muon beam with a central momentum that can be chosen in the range 100-300 MeV/c,
2. an experimental area that can accommodate a cooling and instrumentation setup of initially $\sim$ 30 m in length, and eventually up to $\sim$ 50 m in length, and
3. instrumentation to precisely measure the positions of the incoming and outgoing particles in 6-D phase space and confirm that they are muons.

In the initial design shown in Fig. 37, the instrumentation consists of identical measuring systems before and after the cooling apparatus [173]. Each measuring system consists of (a) an upstream time measuring device to determine the arrival time of the particles to one quarter of an rf cycle ($\sim \pm$300 ps), (b) an upstream momentum spectrometer in which the track trajectories are measured by low pressure TPC's on either side of a bent solenoid, (c) an accelerating rf cavity to change the particles momentum by an amount that depends on its arrival time, (d) a downstream momentum spectrometer, which is identical to the upstream spectrometer, and together with the rf cavity and the upstream spectrometer forms a precise time measurement system with a precision of a few ps. The measuring systems are 8 m long, and are contained within a high-field solenoidal channel to keep the beam particles within the acceptance of the cooling apparatus.

It is proposed to accomplish this ionization cooling R&D program in a period of about 6 years. At the end of this time we believe that it will be possible to assess the feasibility and cost of constructing an ionization cooling channel for the First Muon Collider, and if it proves feasible, begin a detailed design of the complete cooling channel.